DOI: 10.1002/adma.200701466

A Catalytic Reaction Inside a Single-Walled Carbon Nanotube**

By *Hidetsugu Shiozawa,* Thomas Pichler, Alexander Grüneis, Rudolf Pfeiffer, Hans Kuzmany, Zheng Liu, Kazu Suenaga,* and *Hiromichi Kataura*

More than fifteen years after their discovery, single-walled carbon nanotubes (SWCNTs) are still attracting much interest for their novel electronic and structural properties. The interior space of the SWCNTs can be utilized for encapsulation of molecules. This opens the pathway for the exploration of a new chemistry within the confined one-dimensional nanospace inside the tubes. The first example was the encapsulation of fullerenes.[1] Later on fullerene-filled SWCNTs were transformed into double-walled carbon nanotubes (DWCNTs).[2] This demonstrated the non-catalytic growth of the secondary SWCNTs based on the coalescence of adjacent fullerenes tightly encapsulated within the primary SWCNTs. In turn, attempts to fill SWCNTs with other fullerenes, atoms, and molecules have been intensively explored. Very recently, organic molecules encapsulated in SWCNTs have been reported.[3–5] Owing to their large variety with diverse chemical properties, the incorporated organic molecules can tune the properties of the SWCNTs.[3] Aside from being a tuning material for the SWCNT properties, the encapsulated molecules themselves may well exhibit novel structural and chemical properties in the confined nanospaces. It is therefore important to explore such nanochemistry by using various filler molecules and analyze the chemical reactions using state-of-the-art spectroscopic and microscopic techniques.

In the present work, the idea of nanochemistry within SWCNTs is applied to grow the secondary nanotubes from encapsulated ferrocenes ($FeCp_2$), the most stable metallocene. It turns out that the tube growth is a catalytic process that yields iron-doped and nondoped DWCNTs as final products. The filling of SWCNTs with metallocenes has thus far been observed for cobaltocenes ($CoCp_2$)[6] and ferrocenes ($FeCp_2$)[7,8] with high-resolution transmission electron microscopy (HRTEM). Tube-diameter-selective filling and the resulting energy shifts of the corresponding fluorescence peaks were observed for cobaltocene peapods ($CoCp_2$@NT). The HRTEM measurements of $FeCp_2$@NT showed the conversion of the $FeCp_2$ to inner tubes[7] and to iron clusters.[8,9] However, evidence for the filling on a bulk scale as well as a detailed analysis of the inner tube growth process have not yet been reported. Accounting for recently reported bulk SWCNT synthesis from only $FeCp_2$ precursor,[10] it is plausible that the within a tube $FeCp_2$ acts as a catalyst and as a carbon source. In comparison to the noncatalytic process required for the inner-tube growth from fullerenes, the catalytic process within a defined nanospace provides an important clue to the growth mechanism for carbon nanotubes.

In this Communication, we first evidence the bulk-scale synthesis of $FeCp_2$@NT. The filling factor and charge transfer value in the $FeCp_2$@NT are quantitatively derived from photoemission spectroscopy. From resonant Raman spectroscopy we find that DWCNT transformations are possible at annealing temperatures as low as 600 °C. A combined photoemission and resonant Raman study reveals that annealing at different temperatures leads to the selective growth of iron-doped and nondoped DWCNTs. At the early stage of the inner-tube growth, iron carbide nanocrystals appear as a metastable iron phase inside the tubes. They are suggested to be responsible for the catalytic growth. Once the inner tubes have grown at 600 °C, we observe the growth of iron nanoparticles on the outside of DWCNTs. The intensity distribution of inner-tube radial breathing modes (RBM) is identical for all $FeCp_2$@NT-grown DWCNTs but significantly different to the DWCNTs grown from fullerene peapods. This observation is attributed to the catalytic inner-tube growth leading to larger inner-tube–to–outer-tube distances in the $FeCp_2$@NT-grown DWCNTs. This also explains the observed

[*] Dr. H. Shiozawa[+], Dr. T. Pichler[++], Dr. A. Grüneis
IFW Dresden, 01171 Dresden (Germany)
E-mail: h.shiozawa@surrey.ac.uk
Dr. R. Pfeiffer, Prof. H. Kuzmany
Institut für Materialphysik, Universität Wien
Strudlhofgasse 4, 1090 Wien (Austria)
Dr. Z. Liu, Dr. K. Suenaga
Research Center for Advanced Carbon Materials, AIST
Tsukuba 305-8565 (Japan)
Dr. H. Kataura
Nanotechnology Research Institute, AIST
Tsukuba 305-8562 (Japan)
[+] Present address: Advanced Technology Institute, University of Surrey, Guildford GU2 7XH, United Kingdom.
[++] Present address: Institute für Materialphysik, Universität Wien, Strudlhofgasse 4, 1090 Wien, Austria.

[**] H.S. thanks the Alexander von Humboldt foundation. A.G. acknowledges an individual Marie Curie fellowship from the European Union. R.P. acknowledges support from FWF projects P17345 and I83-N20 (ESF IMPRESS). H.K. acknowledges support by the Industrial Technology Research Grant Program in 2003 from the New Energy and Industrial Technology Development Organization (NEDO) of Japan. This work was performed under DFG Pl 440/1/3 and supported in part by a Grant-in-Aid for Scientific Research A (No.18201017) by the Ministry of Education, Culture, Sports, Science, and Technology of Japan. We thank R. Hübel, S. Leger, R. Schönfelder, and H. Klose for technical assistance.

ADVANCED MATERIALS

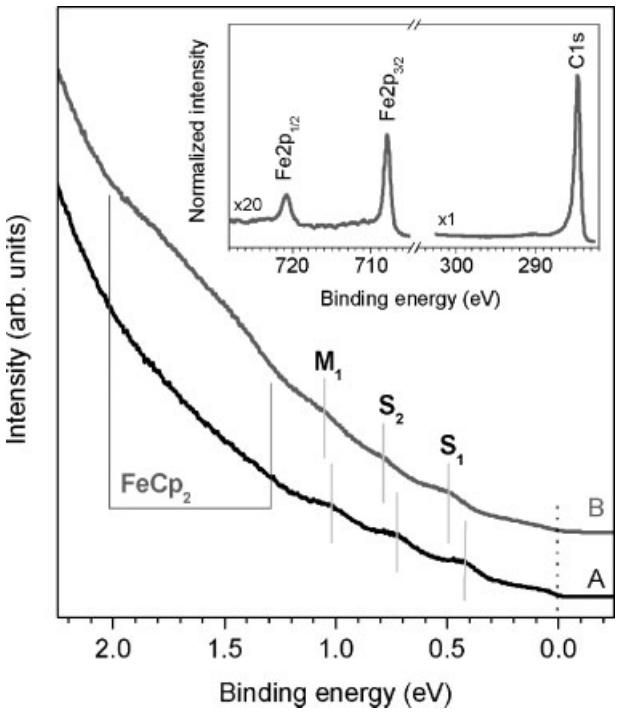

Figure 1. He I photoemission spectra of pristine SWCNTs (spectrum A) and $FeCp_2$@NT (spectrum B). The inset shows the normalized X-ray photoemission spectra of $FeCp_2$@NT at Fe 2p and C 1s edges.

inner-tube growth even at much lower reaction temperatures than for fullerenes. In this way, based on the comprehensive structural and chemical analysis of the reaction process inside the tube this work provides a new route to engineer novel nanomaterials.

The inset of Figure 1 shows the normalized core-level photoemission spectra of the $FeCp_2$@NTs at the C 1s and Fe 2p edges. In the Fe 2p spectrum we observe sharp peaks at 708.0 and 720.8 eV binding energies, corresponding to the Fe $2p_{3/2}$ and Fe $2p_{1/2}$ edges, respectively. These peaks were not observed for the pristine SWCNTs. The spectral shape is very similar to that of $FeCp_2$ molecules sublimed on an Ag substrate.[11] This observation indicates the presence of $FeCp_2$ in the sample on a bulk scale. From the integrated intensity ratio between the Fe 2p and the C 1s peaks, we evaluate the number of iron atoms relative to carbon atoms to be $N_{Fe/C} \sim 0.003$. Assuming that the $FeCp_2$@NT sample consists of nonfilled SWCNTs and filled SWCNTs, and that the latter includes the $FeCp_2$ molecules lying along the tube axis with an adjacent $FeCp_2$ distance of 0.755 nm,[12] we obtain a filling factor of about 35%. This value was well-reproduced in several different filling experiments and thus seems to be an optimum value for the present SWCNT sample.

The detailed analysis of the valence-band electronic structure of the $FeCp_2$@NT in comparison to that of the SWCNTs was performed using ultraviolet photoemission spectroscopy. The valence-band spectra of the pristine SWCNTs and $FeCp_2$@NTs are plotted in Figure 1. For the $FeCp_2$@NT a trapezoidal structure is observed at binding energies ranging from 1.7 to 2.0 eV. This is not observed for the pristine SWCNTs and can be attributed to the highest occupied molecular orbital of the $FeCp_2$. Both spectra exhibit three peaks corresponding to the van Hove singularities (VHS) of semiconducting tubes (S_1, S_2) and metallic tubes (M_1).[13] The VHS peaks for the $FeCp_2$@NT are located at 0.5, 0.8, and 1.1 eV, which means that they are shifted towards higher binding energies in comparison with those of the pristine SWCNTs. This behavior is very similar to what was observed with potassium- or lithium-intercalated SWCNTs,[14,15] and can be confidently attributed to electron doping from the $FeCp_2$ to the SWCNTs. From a comparison to the photoemission results for the potassium-intercalated SWCNTs,[14] we evaluate quantitatively the number of electrons transferred to the SWCNTs. From a linear fit of the energy position of the VHS peaks as a function of the number of potassium atoms, we get the number of electrons transferred from the $FeCp_2$ to the SWCNTs to be $N_C \sim 4.2 \times 10^{-4}$ per nanotube carbon atom. Using $N_{Fe/C} \sim 0.003$ for $FeCp_2$@NT, we get the number of electrons transferred from the $FeCp_2$ to the SWCNTs to be 0.14 electrons per $FeCp_2$. From local-density approximation (LDA) calculations, it has been predicted that the degree of charge transfer in $CoCp_2$@NT is about 0.35–0.55 electrons per $CoCp_2$.[12] The previously reported ionization potential of $FeCp_2$ is 5.88 eV, larger than the value of 4.705 eV of $CoCp_2$.[16] Considering the filling factor of 35% for the present $FeCp_2$@NT sample, the estimated doping level for the $FeCp_2$@NT is very reasonable.

Resonance Raman scattering has been proven to be a valuable tool to analyze the degree of filling by the transformation of filled SWCNTs to DWCNTs. In this case the inner tube RBM response, which correlates to the tube diameters, appears as a set of narrow lines after transformation.[17] Figure 2a exhibits the evolution of the RBM responses for the tube materials upon filling and subsequent vacuum annealing. The Raman spectrum of the $FeCp_2$@NT shows the RBM lines at frequencies ranging from 150 to 200 cm^{-1} which means up-shifted to higher frequencies and broadened as compared to those of the pristine SWCNTs. This is common for molecule-filled SWCNTs.[18] After vacuum annealing at temperatures at and above 600 °C, the $FeCp_2$@NT is successfully transformed into DWCNTs. Examples are shown in Figure 2a with the Raman responses for the $FeCp_2$@NT samples annealed at 600 °C for 2 hours and 1150 °C for 1 hour. For both samples, we clearly see sharp lines in the range of 300–350 cm^{-1} which can be assigned to the RBM signals mainly from the (6,5) and (7,3) inner tubes.[19] They are not observed for the reference SWCNT sample annealed at 1150 °C for 1 hour. This fact gives clear evidence for the success of the $FeCp_2$ filling on a bulk scale.

Figure 2b shows the Fe 2p photoemission responses for the DWCNT samples grown at 600 °C and 1150 °C. It is obvious that the final DWCNT products depend strongly on the growth temperatures. Annealing at 1150 °C removes all the iron atoms, which is observed as the disappearance of the Fe 2p core-level peaks. In contrast, annealing at 600 °C converts the $FeCp_2$@NT into the DWCNTs while keeping the iron atoms within the

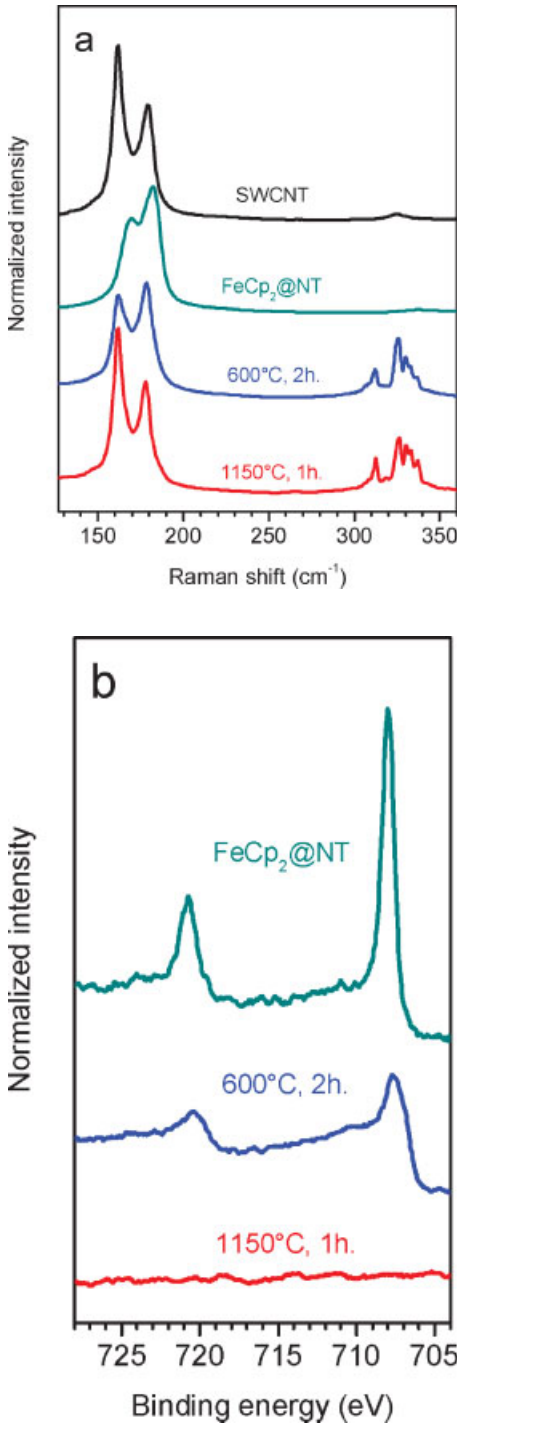

Figure 2. a) Raman spectra in the RBM region for pristine SWCNTs, $FeCp_2$@NT, $FeCp_2$@NT annealed at 600 °C for 2 h and $FeCp_2$@NT annealed at 1150 °C for 1 h. All spectra were recorded with a photon energy (wavelength) of 1.16 eV (1064 nm) at room temperature. b) Fe 2p core-level photoemission spectra for $FeCp_2$@NT and those annealed at 600 °C for 2 h and 1150 °C for 1 h.

tube material. The latter observation demonstrates that the iron-containing DWCNTs were fabricated from the $FeCp_2$@NT. It is noteworthy that the inner tube RBM patterns for the iron-doped ($FeCp_2$@NT annealed at 600 °C for 2 hours) and for the nondoped DWCNTs ($FeCp_2$@NT annealed at 1150 °C for 1 hour) are nearly the same as shown in Figure 2a. This means that the inner tube RBM pattern for the DWCNTs is independent of the observed iron doping.

Further evidence for ferrocene encapsulation and DWCNT growth were obtained from HRTEM observations. Figure 3a shows a HRTEM image of the pristine $FeCp_2$@NT. The image exhibits dark contrasts distributed inside a SWCNT. These were rarely observed outside the tubes and not observed in the pristine SWCNT sample. This demonstrates the successful encapsulation of $FeCp_2$ in the SWCNTs. Figure 3b displays a HRTEM image of the $FeCp_2$@NT sample annealed at 1150 °C for 1 hour, showing a clean DWCNT. Figure 3c–f are HRTEM images of the $FeCp_2$@NT sample annealed at 600 °C for 2 hours. In Figure 3c we find dark contrasts in a tube as observed in Figure 3a, indicating that the molecule units remain inside the tube. Figure 3d is an image of the growing inner tube showing two parallel line contrasts as well as amorphous contrasts inside a SWCNT. Figure 3e shows a tube

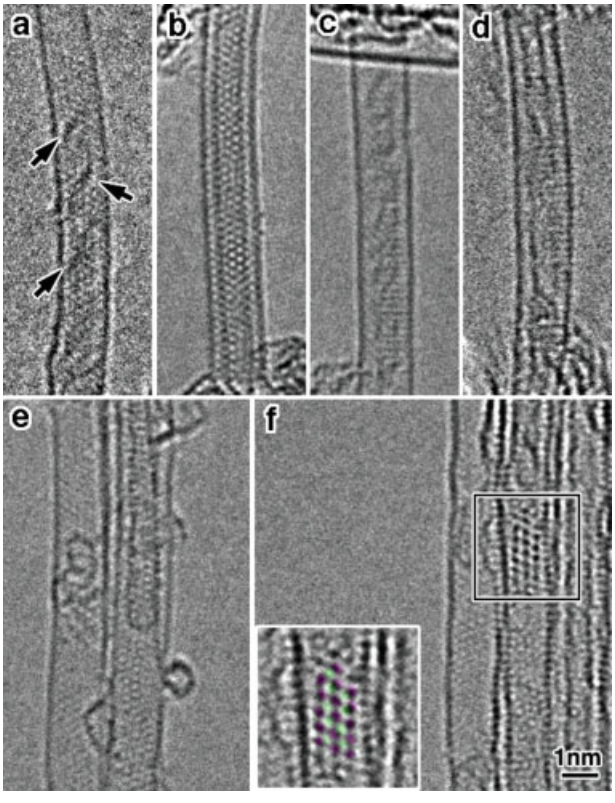

Figure 3. a) TEM image of a pristine $FeCp_2$@NT. Arrows indicate dark contrasts. b) $FeCp_2$@NT annealed at 1150 °C for 1 hour. c–f) $FeCp_2$@NT annealed at 600 °C for 2 hours. The inset of (f) depicts a structure simulation output as purple dots superimposed upon the scaled image of the observed nanocrystal. The lattice of the nanocrystal is well-matched to that of an iron carbide Fe_3C ($a = 0.4523$ nm, $b = 0.5089$ nm, $c = 0.67428$ nm, space group is *Pbnm*).

ADVANCED MATERIALS

containing a capped inner tube. No iron particles with the size of inner tubes were observed at this stage, indicating that the agglomeration of such iron particles is not the mechanism for the inner-tube nucleation and growth. Instead, we found nanocrystals existing inside the SWCNTs such as the one displayed in Figure 3f. From a structure simulation, the lattice of the observed crystals corresponds to that of an iron carbide Fe_3C ($a = 0.4523$ nm, $b = 0.5089$ nm, $c = 0.67428$ nm, space group is Pbnm). From the inset of Figure 3f, it can be seen that the Fe atom columns of the observed nanocrystal, which show black dot contrasts, correspond well to those of Fe_3C showing purple dot contrasts. Such nanocrystals were not observed for the $FeCp_2$@NT sample annealed at 1150 °C for 1 hour. Therefore, it seems that the iron carbides exist only during the inner-tube growth. At high temperatures the reaction is quick, hence, the iron atoms are completely released from the tube material within 1 hour.

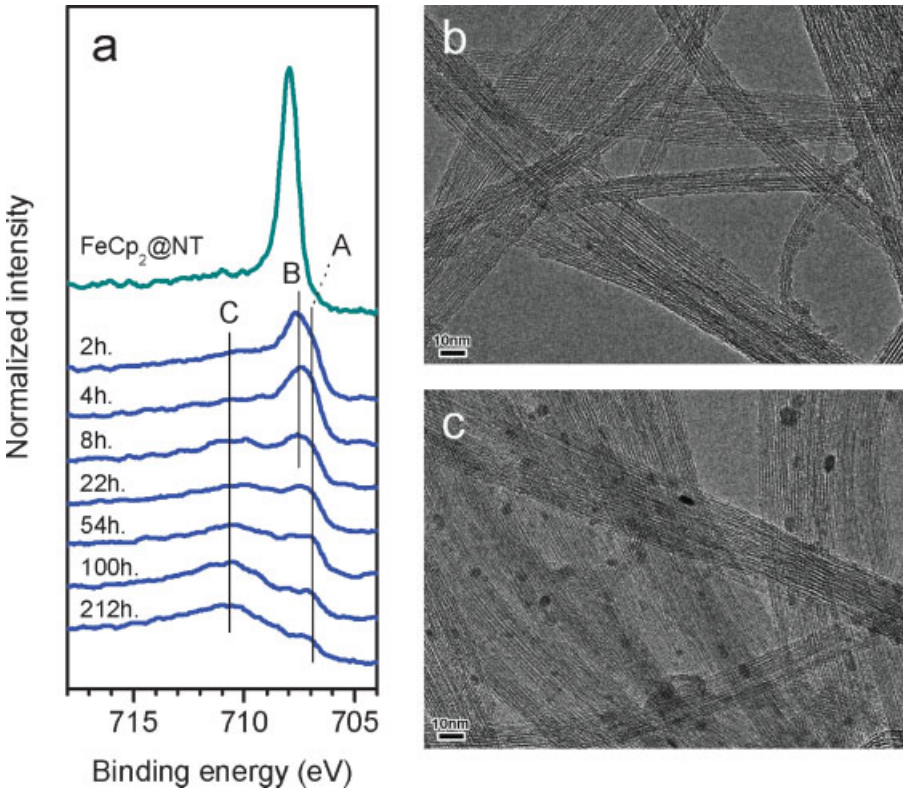

Figure 4. a) Fe 2*p* photoemission spectra of pristine $FeCp_2$@NT and those annealed at 600 °C for 2, 4, 8, 22, 54, 100, and 212 hours. b) TEM image of $FeCp_2$@NT annealed at 600 °C for 2 hours. c) TEM image of $FeCp_2$@NT annealed at 600 °C for 212 hours.

To further investigate the inner tube growth process, the iron chemical properties of the $FeCp_2$@NT samples were traced during the inner-tube growth at 600 °C via the Fe 2*p* photoemission. Figure 4a shows the Fe $2p_{3/2}$ core-level photoemission spectra for the $FeCp_2$@NT samples annealed at 600 °C for 2, 4, 8, 22, 54, 100, and 212 hours. A drastic change in the spectral shape is obvious. After the first 2 hours of annealing the Fe $2p_{3/2}$ peak is broken up into three structures: a main peak, B, located at 707.6 eV; a shoulder, A, at ca. 707 eV; and a broad hump, C, at ca. 710 eV. This obviously reflects a significant change in the chemical environment of the iron atoms and is a clear sign for the decomposition of the $FeCp_2$ within the SWCNTs. The atomic concentration of iron relative to carbon is estimated to be $N_{Fe/C} \sim 0.002$ for the 2 hours annealed sample, showing a loss of Fe atoms of about 25% from the pristine $FeCp_2$@NT sample.

According to the literature, the Fe $2p_{3/2}$ peak of the bulk carbides appears at binding energies of 707.2 eV for Fe_3C[20] and of 706.9 eV or 707.3 eV for Fe_5C_2.[21,22] These values are very close to the value of 707 eV for metallic iron.[23] However, because no metal particles were observed by HRTEM, no pure metallic iron is expected in our sample. Thus, peaks A and B can be assigned to different iron carbide phases. This assignment is also encouraged by the HRTEM observation of the carbide crystals inside the SWCNTs in the $FeCp_2$@NT sample after 2 hours of annealing.

Upon further annealing, peak B disappears after 8 hours, where the Raman response showed the completion of the inner-tube growth. This indicates that the corresponding iron carbide phase is responsible for the inner-tube growth. Peak A decays rather slowly and can be observed even after 212 hours. Moreover, we find that the intensity of peak C increases with decreasing intensity of peak A. The atomic concentration of iron relative to carbon is almost constant for the samples annealed more than 2 hours. Therefore, it is probable that the iron carbide phase appearing as peak A is thermodynamically metastable at 600 °C and gradually transforms into a stable iron state appearing as peak C upon long-term annealing. This point is further analyzed by HRTEM. Figure 4b and c show HRTEM images for the samples annealed at 600 °C for 2 hours and 212 hours. Interestingly, black dot contrasts corresponding to iron particles with diameters ranging from 2 to 5 nm are observed only after 212 hours of annealing. Most of them seem to be located outside the tubes. This observation indicates that after the inner-tube growth the iron atoms diffuse out of the tubes and aggregate into nanoparticles, as illustrated in Figure 5. This process is of course accompanied by changes in the iron chemical environments that determine the evolution of the spectral weights between the A and C peak components in the Fe 2p photoemission.

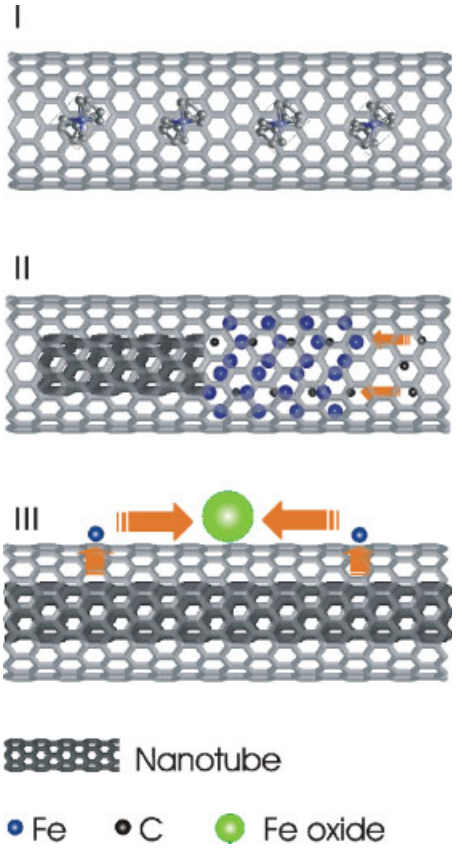

Figure 5. Schematic diagram for the inner tube growth process. I) $FeCp_2$-filled SWCNTs. II) Catalytic reaction for the inner-tube growth after decomposition of $FeCp_2$. The iron carbide nanocrystal acting as a reactor absorbing carbon atoms from one side and generating a nanotube to another side. III) Precipitation of iron atoms onto the DWCNT surface and subsequent oxidation and aggregation into a nanoparticle.

Peak C can be assigned to oxidation states of iron.[23] However, in comparison to the usual divalent or trivalent iron compounds the observed peak C is much broader and asymmetric. A broad core-level spectrum is generally due to a strong mixture between the Fe 3*d* states and corresponding ligands. Additionally, the asymmetry of the core level photoemission peak can be due to the mixing of the 3d states with surrounding continuum states, that is, the metallic states of the SWCNTs. Therefore, the unusually broad and asymmetric Fe 2p photoemission peaks indicate a strong interaction between the Fe 3d electrons of the observed nanoparticles and the conduction electrons of the SWCNTs. These features should appear only when the iron atoms form very small clusters and closely adhere to the tube walls. This is exactly the case observed by HRTEM and is of future interest as a template for exploring exotic magnetic properties in well-defined nanoparticles.[24–26]

In the following we analyze the DWCNT products from the $FeCp_2$@NT in comparison to the DWCNTs grown from the C_{60}@NT by using high-resolution resonant Raman spectroscopy. All samples were prepared from the same batch of SWCNT film to exclude any changes arising from the different diameter distributions of the outer tubes. An example is given as spectrum A in Figure 6a for the C_{60}@NT-grown DWCNTs recorded with an excitation energy (wave length) of 2.10 eV (590 nm). For this laser the inner tubes with chirality (6,4) and (6,5) are close to resonance with E_{22}^{S} and appear as a set of lines between 300 and 365 cm^{-1}. Each line corresponds to a (6,4) or (6,5) tube inside different outer tubes. The smaller the outer-tube diameter the higher is the RBM frequency of the inner tube due to tube-tube interaction.[17,19] Each peak can be assigned to a well-defined inner tube-outer tube pair. As an example, the peak labelled (13,6) is the response from a (6,4) tube inside a (13,6) tube. The inner tube-outer tube diameter difference for this pair is 0.63 nm. In this way diameter differences can be evaluated for all tube pairs. The broad peak assigned as S and extending from 331 to 333 cm^{-1} originates from (6,4) tubes in several rather large outer tubes with diameter differences between 0.715 and 0.743 nm. Even in this case, in spite of the strong overlap, the outer tubes are well defined.

Comparing the spectral pattern for the inner tube grown from the C_{60} with that for the inner tube grown from the $FeCp_2$ yields several surprising results. The corresponding spectra are depicted in Figure 6a. Firstly, the line positions are exactly the same in both cases which means the same assignment to tube pairs can be used. Secondly, the intensity distribution for the various tube pairs is significantly different for the C_{60}-grown inner tubes and for the $FeCp_2$-grown inner tubes. In the latter case the (6,4) tubes in the rather large outer tubes are clearly dominating. Thirdly, this feature is independent of the annealing temperature as compared between 600 and 1150 °C in Figure 2a, which means the same growth mechanism is relevant for the both cases and it is different from that for the C_{60} precursor.

Additionally, in the present work using various excitation energies in the range of 1–2.5 eV no RBM lines for the C_{60}-grown inner tubes were observed beyond the (6,4) tube, reflecting the corresponding tube diameter of 0.69 nm is the smallest for the C_{60}-grown inner tubes. This is not the case for the $FeCp_2$@NT-grown DWCNTs where we could observe smaller-tube RBM lines with frequencies as high as 465 cm^{-1}. The highest frequency peak was located at 465 cm^{-1} with the excitation energy of 2.41 eV. It corresponds to (6,0) and (4,3) tubes with diameters around 0.485 nm. Using a typical van der Waals distance of 0.34 nm as an intra-tube distance for the DWCNTs, we estimate the outer-tube diameter for the $FeCp_2$@NT to be as small as 1.165 nm which is much smaller than for the C_{60} peapods.[27] This peak was observed only for the DWCNT sample grown at 600 °C and did not appear for the DWCNT sample grown at 1150 °C. It demonstrates that very small inner tubes can be grown only at the moderate temperature of 600 °C.

Before we start further discussion we recall that in the above described experiments we always study the response from a certain type of inner tube encapsulated in different outer tubes. This means the resonance cross section remains almost always

ADVANCED MATERIALS

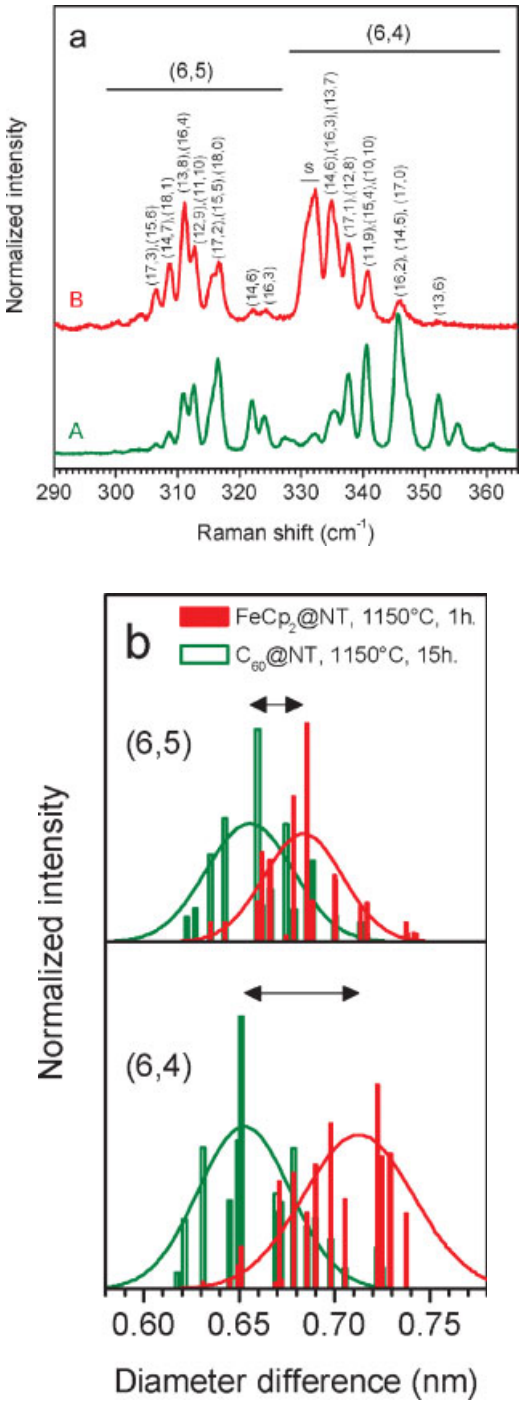

Figure 6. a) High-resolution Raman responses recorded at a photon energy (wavelength) of 2.10 eV (590 nm) for the (6,5) and (6,4) inner tubes grown from C_{60} (spectrum A) and for those from $FeCp_2$ at 1150 °C (spectrum B). b) RBM line intensity versus inner tube-outer tube diameter difference for the DWCNTs with (6,5) and (6,4) inner tubes. The solid curves are from Gaussian fits of the corresponding inner-tube RBM intensities.

the same and the observed line patterns represent real pair occupation probabilities. Moreover, the spectral patterns for the $FeCp_2$@NT-grown DWCNTs were well reproduced with the DWCNTs grown from $GdCp_3$-filled SWCNTs. Therefore, it seems that the fine structures of the inner-tube RBM are identical among the DWCNTs from different metallocene-filled SWCNTs. Since the $GdCp_3$ comprising of three planar aromatic ligands around a gadolinium ion shows the same spectral feature as of the $FeCp_2$ comprising of two planar aromatic ligands around an iron, the shape of the inner-tube RBM seems to be independent of the structural form and the number of carbon atoms in the precursor material.

Figure 6b shows the RBM line intensity versus inner tube-outer tube diameter difference of the corresponding DWCNTs, clearly describing the fact that the mean diameter difference is larger for the $FeCp_2$@NT-grown DWCNTs. Moreover, the difference between the $FeCp_2$@NT-grown and C_{60}@NT-grown DWCNTs is larger for the (6,4) inner tubes than for the (6,5) inner tubes as indicated by horizontal arrows. For the $FeCp_2$@NT-grown DWCNTs, it seems that the diameter difference increases with decreasing tube size. In contrast, for the C_{60}@NT-grown DWCNTs the diameter difference is similar for the (6,4) tubes and (6,5) tubes and most of those DWCNTs have a diameter difference smaller than that expected from the typical van der Waals distance for graphite. The characteristically different line distributions for the C_{60}@NT-grown DWCNTs and the $FeCp_2$@NT-grown DWCNTs suggest two significantly different growth mechanisms for the two cases. The presence of the Fe_3C nanocrystals as observed by the HRTEM and photoemission measurements suggests, that these crystals act as a catalyst. At the moderate temperature of 600 °C (and of course also at 1150 °C) the $FeCp_2$ decomposes and Fe_3C nanocrystals grow. The liberated carbon particles dissolve in the carbide and eventually precipitate from there to form the inner-shell tube, as illustrated in Figure 5. Since in this process each inner tube is grown from scratch, the diameter can be well adapted to the outer-tube diameter and an optimum diameter difference can be established. This was (0.72 ± 0.02) nm for the (6,4) tubes and (0.68 ± 0.02) nm for the (6,5) tubes. In contrast, in the case of C_{60} precursor predefined caps of the growing inner tubes are available which apparently have a strong influence on the diameter of the eventually grown inner tubes. So, as in our case, the (6,4) tubes with a diameter of 0.69 nm that is smaller than the C_{60} diameter of 0.70 nm grow with great preference also in narrower outer tubes. The narrowing of the already existing cap is possible but takes serious effort. The diameter of the (6,5) tube is 0.75 nm that is larger than the diameter of C_{60}. In this case, the inner-tube diameter is closer to the optimal size, hence, the diameter difference is more similar to that for the $FeCp_2$@NT-grown DWCNTs, as can be seen in Figure 6b.

In summary, we have demonstrated new chemistry using SWCNTs as a nanometer-scale reaction furnace. A comprehensive analysis using state-of-the-art spectroscopic and microscopic techniques unravelled the catalytic pathway of the inner-tube growth from the encapsulated ferrocene precursor. The final products are iron-based nanoparticles residing on DWCNTs with a well-defined intra-tube spacing and doping level. Such nanocomposites have great potential as functional

templates for proving the concepts of nanometer-scale physics, molecular electronics, and biomedical applications. Hence, this confined catalytic process represents a new route for materials design.

Experimental

SWCNTs with diameters in the range of (1.4 ± 0.1) nm were synthesized by laser ablation and purified by H_2O_2 treatment[13,18]. The tube material was then prepared to bucky film and the endcaps were opened by annealing at 450 °C in air. The filling of the SWCNTs with $FeCp_2$ was performed by exposing the open-ended SWCNT bucky film to the vapor phase of $FeCp_2$ at 70–150 °C for several days in a sealed Pyrex-glass ampule. After the filling reaction, the bucky film was dissolved in acetone solution and filtered more than five times to remove the excess $FeCp_2$. The conversion of the $FeCp_2$@NT to the DWCNTs was carried out via annealing at 600 °C and 1150 °C a vacuum better than 10^{-7} mbar. HRTEM was performed with JEM-2010F equipped with a Cs corrector at an accelerating voltage of 120 kV. The Raman spectra were recorded at room temperature using a Brucker FT Raman spectrometer with an excitation energy (wavelength) of 1.16 eV (1064 nm) and at 80 K using a Dilor XY triple spectrometer with 1.84 eV (676 nm) and 2.10 eV (590 nm). For the photoemission measurements, the prepared films were transferred into a photoemission chamber and cleaned by annealing at 350 °C before measurements. The X-ray and ultraviolet photoemission spectra were collected with monochromatic Al Kα radiation (1486.6 eV) and He I radiation (21.22 eV), respectively, using a hemispherical SCIENTA SES 200 photoelectron energy analyzer. The experimental resolution and the Fermi energy were determined from the Fermi edge of clean Mo substrates. The overall energy resolutions were better than 20 meV for ultraviolet and 450 meV for X-ray photoemission. The base pressure in the setup was kept below 5×10^{-10} mbar.

Received: June 19, 2007
Revised: November 9, 2007

[1] B. W. Smith, M. Monthioux, D. E. Luzzi, *Nature* **1998**, *396*, 323.
[2] S. Bandow, M. Takizawa, K. Hirahara, M. Yudasaka, S. Iijima, *Chem. Phys. Lett.* **2001**, *337*, 48.
[3] T. Takenobu, T. Takano,1 M. Shiraishi, Y. Murakami, M. Ata, H. Kataura, Y. Achiba, Y. Iwasa, *Nat. Mater.* **2003**, *2*, 683.
[4] Y. Fujita, S. Bandow, S. Iijima, *Chem. Phys. Lett.* **2005**, *413*, 410.
[5] K. Yanagi, Y. Miyata, H. Kataura, *Adv. Mater.* **2006**, *18*, 437.
[6] L. J. Li, A. N. Khlobystov, J. G. Wiltshire, G. A. D. Briggs, R. J. Nicholas, *Nat. Mater.* **2005**, *4*, 481.
[7] L. Guan, Z. Shi, M. Li, Z. Gu, *Carbon* **2005**, *43*, 2780.
[8] Y. Li, R. Hatakeyama, T. Kaneko, T. Okada, *Jpn. J. Appl. Phys.* **2006**, *45*, L428.
[9] Y. Li, R. Hatakeyama, T. Kaneko, T. Okada, T. Kato, *Nanotechnology* **2006**, *17*, 4143.
[10] A. Barreiro, S. Hampel, M. H. Rummeli, C. Kramberger, A. Gruneis, K. Biedermann, A. Leonhardt, T. Gemming, B. Buchner, A. Bachtold, T. Pichler, *J. Phys. Chem. B* **2006**, *110*, 20973.
[11] C. M. Woodbridge, D. L. Pugmire, R. C. Johnson, N. M. Boag, M. A. Langell, *J. Phys. Chem. B* **2000**, *104*, 3085.
[12] V. M. Garcia-Suarez, J. Ferrer, C. J. Lambert, *Phys. Rev. Lett.* **2006**, *96*, 106804.
[13] H. Ishii, H. Kataura, H. Shiozawa, H. Yoshioka, H. Otsubo, Y. Takayama, T. Miyahara, S. Suzuki, Y. Achiba, M. Nakatake, T. Narimura, M. Higashiguchi, K. Shimada, H. Namatame, M. Taniguchi, *Nature* **2003**, *426*, 540.
[14] H. Rauf, T. Pichler, M. Knupfer, J. Fink, H. Kataura, *Phys. Rev. Lett.* **2004**, *93*, 096805.
[15] R. Larciprete, L. Petaccia, S. Lizzit, A. Goldoni, *Phys. Rev. B* **2005**, *71*, 115435.
[16] C. Cauletti, J. C. Green, M. R. Kelly, *J. Electron Spectrosc. Relat. Phenom.* **1980**, *19*, 327.
[17] R. Pfeiffer, F. Simon, H. Kuzmany, V. N. Popov, *Phys. Rev. B* **2005**, *72*, 161404(R).
[18] H. Kataura, Y. Maniwa, M. Abe, A. Fujiwara, T. Kodama, K. Kikuchi, H. Imahori, Y. Misaki, S. Suzuki, Y. Achiba, *Appl. Phys. A* **2002**, *74*, 349.
[19] V. N. Popov, *New J. Phys.* **2004**, *6*, 17.
[20] I. N. Shabanova, V. A. Trapeznikov, *J. Electron Spectrosc. Relat. Phenom.* **1975**, *6*, 297.
[21] D. J. Dwyer, J. H. Hardenbergh, *Appl. Surf. Sci.* **1984**, *19*, 14.
[22] J. B. Butt, *Catal. Lett.* **1990**, *7*, 61.
[23] *Handbook of X-Ray Photoemission Spectroscopy* (Eds: J. F. Moulder, W. F. Strickle, P. E. Sobol, K. D. Bomben), Perkin-Elmer, Eden Prairie, MN **1992**.
[24] T. W. Odom, J.-L. Huang, C. L. Cheung, C. M. Lieber, *Science* **2000**, *290*, 1549.
[25] Y. Yamamoto, T. Miura, M. Suzuki, N. Kawamura, H. Miyagawa, T. Nakamura, K. Kobayashi, T. Teranishi, H. Hori, *Phys. Rev. Lett.* **2004**, *93*, 116801.
[26] K. Yakushiji, F. Ernult, H. Imamura, K. Yamane, S. Mitani, K. Takanashi, S. Takahashi, S. Maekawa, H. Fujimori, *Nat. Mater.* **2005**, *4*, 57.
[27] H. Shiozawa, H. Ishii, H. Kihara, N. Sasaki, S. Nakamura, T. Yoshida, Y. Takayama, T. Miyahara, S. Suzuki, Y. Achiba, T. Kodama, M. Higashiguchi, X. Y. Chi, M. Nakatake, K. Shimada, H. Namatame, M. Taniguchi, H. Kataura, *Phys. Rev. B* **2006**, *73*, 075406.